As originally published in the SMTA Proceedings.

The Effect of Sb and Ag Addition on the Melting, Undercooling and Mechanical Behavior of Sn-Bi LTS

Yifan Wu, Hannah Fowler, Nathaniel Weddington, Sean Yenyu Lai, Sukshitha Achar Puttur Lakshminarayana, Ganesh Subbarayan-Shastri, John Blendell
Purdue University
IN, USA
wu1394@purdue.edu

ABSTRACT
Low temperature solders based on Sn-Bi are used as substitutes for Sn-Ag-Cu (SAC) alloys, reducing reflow temperature and, hence, warpage-induced defects. Understanding the effects of microalloying elements on solder mechanical, microstructural, and thermodynamic properties is an essential part of alloy design. This study focuses on the changes in melting and solidification behavior of near-eutectic Sn-Bi alloys with Sb (0.5-2wt%) and Ag (0-1wt%) additions, and microstructure evolution and intermetallic compound (IMC) growth during isothermal aging at 85°C. Our DSC studies show that, while Sb increases the alloy melting temperature, it also reduces undercooling. This reduction in undercooling is largest for 2wt%Sb alloys in which large SnSb IMCs serve as nucleating sites for Sn dendrites producing a 4˚C undercooling. We discuss these results in light of the observed changes in mechanical properties with isothermal aging of Sb and Ag-containing alloys in thermal cycling performance of the Sn-Bi alloy solder joints.

Key words: Sn-Bi LTS, microalloying, thermodynamics, mechanical properties

INTRODUCTION

The widespread use of SAC alloys following the EU ban of lead-free solders has become increasingly of concern due to their high melting point (217°C). As the microelectronic industry moves towards miniaturization and heterogeneous integration, the high reflow temperature of SAC alloys can cause warpage-induced defects, including head-on-pillow, head-on-pillow open, and bridging, to the solder joints.[1] Consequently, there is an imperative to find lower melting point lead-free alternatives to SAC alloys.

Of particular interest in the realm of low-temperature soldering are alloys based on eutectic Sn-Bi alloys due to the low melting temperature (138°C) and the cost-effectiveness of the eutectic Sn-Bi alloy. Low temperature solders based on Sn-Bi eutectic (LTS) perform well during thermal cycling, however, the strain rate sensitivity of Sn-Bi alloys raises concerns over the mechanical reliability of the alloy, especially when used for high strain rate applications. Following the success and insights gained in improving the mechanical properties of SAC alloys through microalloying, [2, 3] numerous research efforts have been directed towards improving the mechanical performance of Sn-Bi alloys by adding various elements. [4–10] Notably, the addition of silver (Ag) introduces Ag_3Sn IMCs into the solder, leading to a refinement of the microstructure and the strengthening of the alloy.[7, 8] The introduction of copper (Cu) has also demonstrated the ability to refine the solder's microstructure through the formation of Cu_6Sn_5 compounds within the matrix. Various other elements, including zinc (Zn), nickel (Ni), indium (In), antimony (Sb), cobalt (Co), and gold (Au), have been investigated for their impact on IMC growth at the solder-Cu surface finish interface. Detailed insights into these microalloying effects in Sn-Bi solders can be found in the comprehensive review conducted by Wang et al. [11]

The ability of Sb to enhance the ductility of Sn-Bi alloys while preserving their tensile strength has been reported in several studies.[4, 6, 7, 10, 13] These studies suggest that the observed improvement in mechanical properties can be attributed to a dual mechanism: Sb in solid solution in Sn and precipitation of SnSb IMC particles at the β-Sn-Bi interphase boundaries.[5] In this research, we focus on investigating near-eutectic Sn-Bi alloys with Sb and Ag addition to elucidate the relationship between microalloying elements, the melting and solidification characteristics of these solder alloys, and their relationship with the resulting microstructure. Furthermore, we also examine the changes in mechanical properties during isothermal aging of Sb and Ag-containing Sn-Bi alloys, providing insight into the microalloying effect of Sb on mechanical properties. Isothermal aging of solders enables microstructure coarsening and intermetallic growth, depending on the annealing temperature and time. The evolution of LTS solder microstructures and their microstructure stability can have implications about the reliability of the solder joint over time and under different loading conditions.

EXPERIMENTAL

The Scientific Alloys Corporation fabricated a series of six Bi-42Sn-Sb-*y*Ag (*x*=0.5, 1, 2 and *y*=0, 1) solder alloys in the form of 500 µm spheres.[5] Inductively coupled plasma mass spectroscopy (ICP-MS) was used to affirm the alloy compositions prior to other testing. The exact elemental composition of each alloy obtained from ICP-MS is shown in Table 1. Overall, all alloys (except for the Bi-42Sn-2Sb-1Ag alloy) contain more Sn (± 2 wt%) and less Bi (± 2 wt%) than the desired compositions. In terms of microalloying

elements, the concentrations of Sb are close to what is expected (± 0.1 wt%), while the concentration of Ag showed greater variability (± 0.3 wt%).

The thermodynamic properties of the alloys were first investigated using Thermo-Calc (database TCSLD4.2). A TA Q2000 DSC was used to measure the melting and solidification behavior of the alloys. Each testing pan contains a single solder sphere to avoid multiple peaks appearing upon solidification. The following DSC procedure was used for all the testing: equilibrate at 60°C; ramp to 200°C with a ramp rate of 20°C/min; isothermally hold at 200°C for 5 minutes (to ensure complete melting/dissolution of IMCs); ramp down to 60°C at a ramp rate of 20°C/min. For each alloy composition, three separate samples were tested for three DSC cycles each to ensure repeatability.

Solder spheres were extracted at different intervals (1 cycle and 3 cycles) and mounted in epoxy for microstructural analysis. Metallographic samples were mechanically polished to a final polish of 0.05 µm diamond suspension and were imaged using a FEI Quanta 650 FEG scanning electron microscope. As-received solder spheres of each alloy composition were similarly prepared for microstructural analysis. Energy Dispersive X-ray Analysis (EDS) and electron probe microanalysis (EPMA)- wavelength dispersive spectroscopy (WDS) were used to measure the composition of the IMC phases and visualize the distribution of elements and phases across the microstructure.

Open-face sandwich samples, where solder balls are placed on a ball grid array (BGA) test board with an OSP surface finish and only undergo one reflow, were used for the isothermal aging study. The samples were held at 85C to determine the Cu6Sn5 intermetallic layer growth and to observe how the microstructure coarsened over time. Three alloys were used in the aging study: 42Sn-Bi-1Ag, 42Sn-Bi-0.5Sb-1Ag, and 42Sn-Bi-1Sb-1Ag. For mechanical testing, BGA-style test boards were assembled to form 8 solder joints (2 diagonally on each corner). The configuration of the test sample was a two-board sandwich structure with both sides being FR4 printed circuit boards with mask-defined pads and an organic solderability preservatives (OSP) surface finish. The pads of one board were fluxed, the 8 solder spheres were hand placed on the 8 pads, and the first board of each structure was reflowed in a DDM Novastar GF-12HC-HT tabletop reflow oven with a peak reflow temperature of 180°C. After cooling, more flux was added to the solder balls, the second board was placed on top of the first board, and reflowed as before, Monotonic shear testing was performed with a custom mechanical tester on the as-reflowed and isothermally aged (85°C, 10 days) samples at a test temperature of 30°C and a displacement rate of 0.2 µm/s. Each board side was superglued to a metal arm of the mechanical tester so that the two-board sandwich structure is between the two metal arms and then the boards are pulled so that the solder joints were sheared.[14] The maximum strain of the mechanical tester is 0.16 and so the solder joints could not be tested to failure. Six alloy compositions were chosen for the monotonic testing: eutectic Sn-Bi, 42Sn-Bi-0.5Sb, 42Sn-Bi-1Sb, 42Sn-Bi-1Ag, 42Sn-Bi-0.5Sb-1Ag and 42Sn-Bi-1Sb-1Ag. After the mechanical testing, samples were mounted in epoxy and prepared for microstructural characterization with the SEM (Scanning Electron Microscope).

RESULTS AND DISCUSSION

Thermodynamic Analysis of the Alloys

The elemental composition of each alloy obtained from ICP-MS is shown in Table 1. Overall, all alloys contain more Sn and less Bi (except for the Bi-42Sn-2Sb-1Ag alloy) than their nominal compositions. In terms of microalloying elements, the concentrations of Sb are close to what is expected, while the concentration of Ag showed greater variability.

Table 1. Expected solder sphere compositions of Bi-42Sn-xSb-yAg (x = 0.5, 1, 2 and y = 0 or 1) versus the measured results from ICP-MS. [5]

42SnBi-*x*Sb-*y*Ag Alloys		Sn	Bi	Sb	Ag
0.5Sb	Expected	42	57.5	0.5	0
	Measured	43.1	56.5	0.4	0
1Sb	Expected	42	57	1	0
	Measured	43.3	55.7	1.0	0
2Sb	Expected	42	56	2	0
	Measured	43.7	54.3	2.0	0
0.5Sb-1Ag	Expected	42	56.5	0.5	1
	Measured	44.5	53.9	0.6	1.1
1Sb-1Ag	Expected	42	56	1	1
	Measured	42.7	55.5	1.0	0.7
2Sb-1Ag	Expected	42	55	2	1
	Measured	42.2	55.1	1.9	0.7

To aid the understanding of the microalloying effect of Sb on Sn-Bi alloy, calculated phase diagram (CALPHAD) method was employed using the Thermo-Calc software. The calculated liquidus projection of the Sn-Bi-Sb ternary phase diagram is shown in Figure 1 (zoomed into the near-eutectic composition to show the microalloying effect of Sb). The three dots correspond to 0.5, 1 and 2 wt% Sb addition to the eutectic Sn-Bi alloy. The 0.5 Sb addition falls within the (Bi) primary phase field, while the 1 wt% and 2 wt% Sb addition fall within the SnSb phase field. Similarly, in the calculated Scheil solidification paths (Figure 2), Bi is shown to the first phase to nucleate with 0.5 wt% Sb addition. With 1 or 2 wt% addition, SnSb was calculated to be the first phase to solidify in the alloy.

From the liquidus projection and Scheil solidification paths calculation, one would expect a distinct microstructural difference as the Sb concentration increases from 0.5 wt% to 1 wt%. From these calculations, 0.5 wt%Sb would be well within the solid solubility limit in the (Sn) phase and no SnSb should form in the 0.5 wt% Sb sample. Between the 1 wt%

and 2 wt% Sb samples, the calculations show that SnSb forms first from the melt. For the 1 wt% Sb alloy, the SnSb solidification is followed by a Bi + SnSb solidification starting at 141.8°C, eventually leading to the eutectic solidification of Bi + (Sn) at 139.0°C. For the 42Sn-Bi-2Sb composition, SnSb starts solidifying at 179.1°C and ceases at 141.8°C, where the sole solidification of Bi begins. After the mole fraction of the solid reaches 0.01, the solidification of SnSb resumes together with Bi. At 139°C, the eutectic solidification of Bi + (Sn) begins. From the differences in the temperature range and the sequence of the SnSb solidification, one can expect a difference in the SnSb IMC morphology between the 1 wt% and 2 wt% Sb samples. These calculations results are compared with metallographic observations shown in the next section.

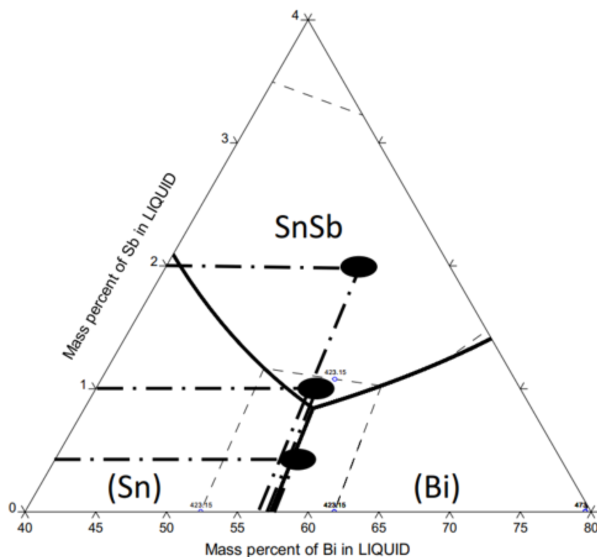

Figure 1. Liquidus projection of the Sn-Bi-Sb ternary phase diagram using the Thermo-Calc database TCSLD4 v4.2. [15]

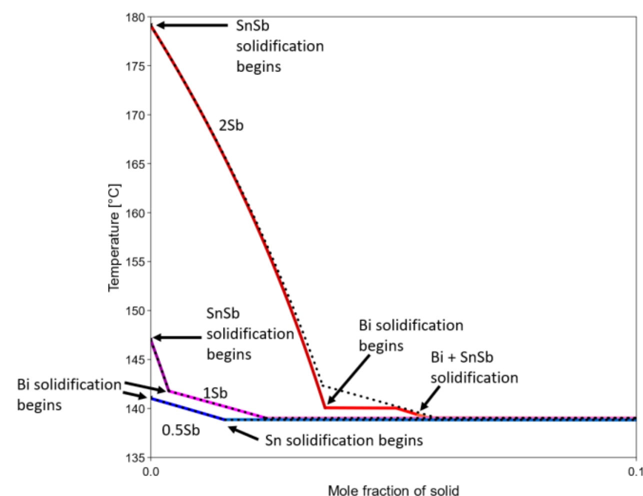

Figure 2. Scheil solidification paths for 42Sn-Bi-xSb (x=0.5, 1, 2) alloys using the Thermo-Calc database TCSLD4 v4.2. [15]

DSC Measurements

Table 2 shows the DSC results of the alloys tested. As the melting and solidification temperatures are identical between Cycle 2 and 3, only results from Cycle 1 and 2 are listed. Based on the melting and solidification temperatures listed, two trends, the changes in the melting point and the changes in the degree of undercooling, are observed. First, the melting temperature increases with increasing amount of Sb addition, from 136.3°C at 0 wt% Sb addition to 142.8°C at 2 wt% Sb addition. The addition of Ag into the binary eutectic Sn-Bi alloy increases the melting temperature to 138.2°C, while the addition of Ag into Sn-Bi-Sb ternary alloys slightly lowers the liquidus temperature. In terms of the degree of undercooling, it decreases from 15°C at 0 wt% Sb addition to a mere 4°C at 2 wt% Sb addition. The addition of Ag into the ternary alloys again shows a less pronounced effect on the degree of undercooling.

Table 2. Melting and solidification temperatures of Bi-42Sn-xSb-yAg (x = 0, 0.5, 1, 2 and y = 0 or 1) alloys [17]

	0Sb0Ag	0.5Sb	1Sb	2Sb	0Sb-1Ag	0.5Sb-1Ag	1Sb-1Ag	2Sb-1Ag
Melting temperature: Cycle 1 (°C)	136.3	139.9	140.8	142.8	138.2	139.3	139.9	141.5
Solidification temperature: Cycle 1 (°C)	121.0	125.0	130.5	138.6	123.9	126.9	131.1	137.6
Degree of Undercooling: Cycle 1 (°C)	15.3	14.9	10.3	4.2	14.3	13.6	8.8	3.9
Melting temperature: Cycle 2 (°C)	136.1	138.5	138.8	138.7	138.0	137.7	137.8	137.9
Solidification temperature: Cycle 2 (°C)	121.0	127.2	132.9	138.7	124.1	127.8	130.1	137.9
Degree of Undercooling: Cycle 2 (°C)	15.1	11.3	5.9	0	13.9	9.9	7.7	-0.1

Upon closer examination of the DSC results, one would also notice a consistent difference between the initial melting point and the melting points of subsequent cycles across all alloy composition, shown in Figure 3 of the Bi-42Sn-2Sb sample. After the initial melting-solidification cycle, the melting point of the sample would decrease by different amounts, depending on their compositions (shown in Figure 4). In the extreme case of 2 wt% Sb addition, the 4°C decrease in the melting point, together with the increased solidification temperature, produces a *negative* amount of undercooling in the sample as seen in Figure 3. Moreover, the shape of the melting peak on cycle 1 and subsequent cycles also differs significantly. The change in the onset temperature of the melting peak suggests a change in partitioning of the Sb in the sample between the initial manufacturing condition and after reflow.

In summary, DSC measurements of the Sb- and Ag-containing alloys reveal that Sb addition increases the melting point and decreases the degree of undercooling of the

alloy. The link between the Sb concentration, the degree of undercooling and the resulting as-reflowed microstructure is examined in the microstructure analysis. An unexpected finding in the DSC study is that a change in the melting temperature was seen between the as-received solder ball samples and the thermal cycled ones. We attempt to account for this phenomenon through microstructural and elemental analysis.

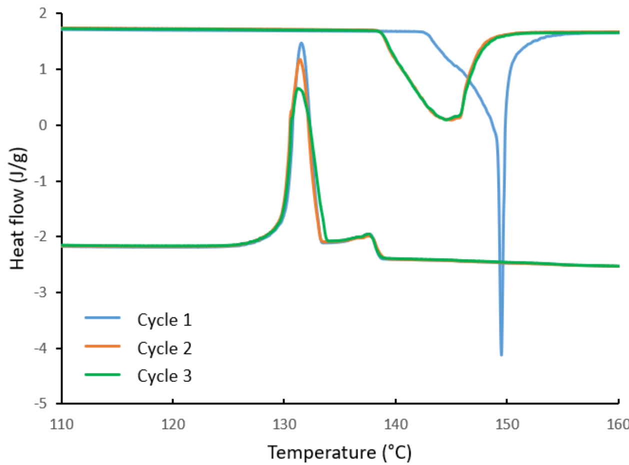

Figure 3. DSC plot of three melting-solidification cycles of the Bi-42Sn-2Sb sample

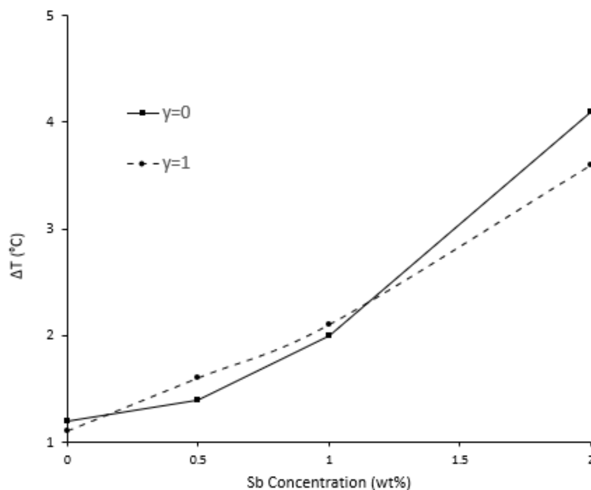

Figure 4. First and second thermal cycle melting temperature difference as a function of Sb concentration in 42Sn-Bi-xSb-yAg alloys

Microstructural Analysis of DSC Tested Samples

The microstructures of samples with 0.5, 1, and 2 wt% Sb are compared in Figure 5, and elemental maps of Sb are compared in Figure 6. Since there's little-to-no difference between samples after 1 and 3 DSC cycles, only samples after 3 cycles are shown and compared with the as-received ones.

0.5 wt% Sb alloy Figure 5a (as-received) and Figure 5g (after 3 DSC cycles) show the microstructure of the Sn-Bi alloy with 0.5 wt% Sb addition. In the as-received solder ball sample in Figure 5g, fine Sn dendrites can be seen throughout the sample. This is in sharp contrast with the microstructure of the as-received sample shown in Figure 5a and 5d, where the microstructure is more homogeneous and much coarser. No intermetallic phases were observed in either of the samples. The lack of IMC is further confirmed in the EPMA elemental maps shown in Figure 6a and 6d. This is also in accordance with the Thermo-Calc calculation results that Bi is the first phase to precipitate upon solidification and that the Sb concentration in this composition is within the solid solubility limited in β-Sn at room temperature.

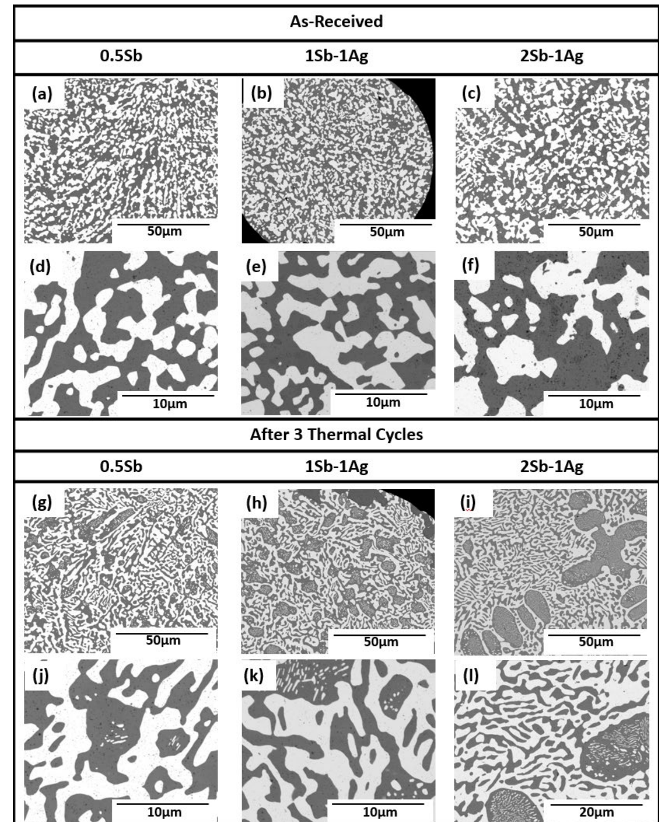

Figure 5. Microstructures of Bi-42Sn-*x*Sb solder alloy (x = 0.5, 1.0, 2.0): (a)-(f) as received liquid-cooled spheres and

(g)-(l) after three thermal cycles at a ramp rate of 20°C/min with microstructures similar to those seen after reflow

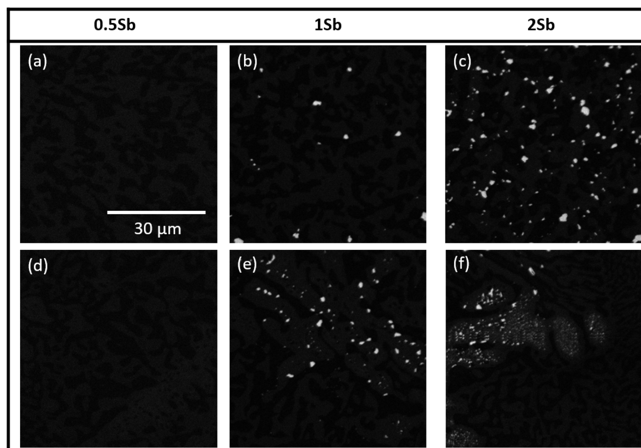

Figure 6. EPMA-WDS maps of the Sb distribution in: (a)-(c) liquid-cooled as-received samples and (d)-(f) samples after thermal cycling in DSC. The 0.5Sb images (a) and (d) show Sb in solution with Sn as a light grey phase. The 1Sb and 2Sb samples (b), (c), (e), and (f) show bright white SnSb IMC particles.

1.0 wt% Sb alloy In samples with 1 wt% Sb addition, similar microstructural changes are seen before and after thermal cycling. What is different from the 0.5 wt% Sb case is that SnSb particles can be seen both in as-received samples and thermal cycled samples, as shown in both Figure 5 and 6. It should be noted that the SnSb IMC particles observed are distributed differently before and after thermal cycling, which can be clearly seen in the EPMA maps. In the as-received sample, fine SnSb particles are dispersed throughout the sample at β-Sn-Bi phase boundaries (Figure 6b). After thermal cycling, SnSb particles are found predominantly within the Sn dendrites (Figure 6e).

2.0 wt% Sb alloy Samples with 2 wt% Sb addition show the most prominent microstructural changes before and after thermal cycling. The as-received microstructure (Figure 5c) is similar to that of the 0.5 and 1 wt% Sb samples, and the EPMA map (Figure 6c) confirms the similar distribution of SnSb particles throughout the as-received sample. However, after thermal cycling, large SnSb IMC particles (>20µm) can be seen near the edge of the sample. The thermodynamic calculation results predict that primary SnSb should be the first phase to solidify during cooling. The presence of a few, large SnSb particles forming around the periphery of the solder joint supports the prediction of primary SnSb. What is also noticeable in the 2 wt% Sb samples is that the Sn dendrites are fewer but much coarser than in the 0.5wt% Sb and 1 wt% Sb alloys. Microstructural cross-sections show that the Sn dendrites appear to have nucleated on the primary SnSb particles, leading to the observed decrease in the degree of undercooling. At lower Sb concentrations, especially at concentrations below 1 wt%, it appears that primary SnSb particles do not form in the melt during cooling and therefore, are not present to act as nucleation agents from the melt.

In summary, the microstructural analysis reveals a clear transition from being SnSb-free at 0.5 wt% Sb addition to having SnSb precipitates within the Sn phase at Sb additions higher than 1 wt%. At higher Sb addition (2 wt%), the SnSb particles are significantly larger in size, since they form as the primary starting at approximately 179°C. The presence of IMC particles provides an explanation for the reduced degrees of undercooling as SnSb can serve as nucleation sites for Sn. The clear difference in the microstructures between the as-received, more rapidly solidified solder spheres and the DSC-cycled solder spheres affords an explanation to the change in the melting point before and after the first DSC cycle. In the fabrication of the solder spheres, the alloys were rapidly quenched into 500µm spheres, while in the DSC cycle the samples were slowly cooled at a constant rate of 20°C/min. The rapid cooling results in a homogeneous microstructure (Figure 4a-f), and likely a supersaturation of Sb in Sn. During the DSC cycle, the alloy was re-melted, and the slower cooling rate during solidification allows sufficient diffusion to take place, thus eliminating the possibility of such supersaturation of Sb in Sn.

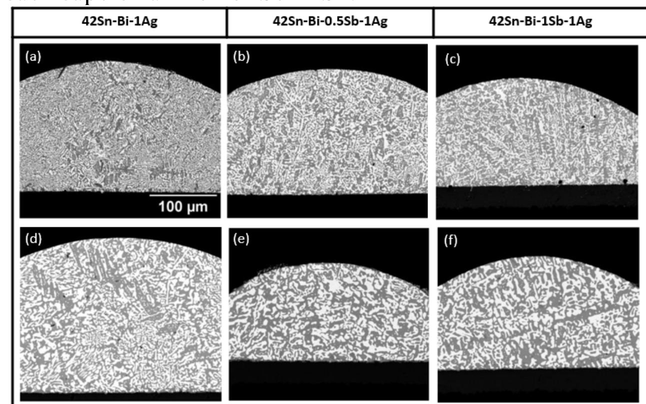

Figure 7. Backscatter SEM images of near-eutectic 42Sn-Bi-xSb-yAg samples with solder reflowed on a BGA test board with an OSP finish: (a)-(c) as-reflowed, and (d)-(f) after 10 days isothermal aging at 85°C.

Mechanical Testing

The microstructure of near-eutectic 42Sn-Bi-xSb-yAg solder joints with OSP finishes are shown in Figure 7. The as-reflowed microstructures show various amounts of Sn dendrites and both coarse and fine eutectic regions. Particles of Ag_3Sn IMC can be seen in samples with Ag additions. With the exception of Cu_6Sn_5 IMC layer formed at the solder-OSP interface, the microstructures of as-reflowed solder joints are similar to the solder spheres after three DSC cycles (Figure 5). After 10 days of isothermal aging at 85°C, both the eutectic structure and Bi precipitates found within the Sn dendrites coarsened. The Cu_6Sn_5 IMC layer also grew in thickness. The Cu_6Sn_5 IMC layer growth rate was higher in the alloys with Sb than in the eutectic 42Sn-Bi-1Ag with the eutectic 42Sn-Bi-1Ag samples showing an average increase from 0.83 µm to 1.22 µm. For the Sb-containing samples, IMC layer thickness increased from 0.83 µm to 1.57 µm for

the 42Sn-Bi-0.5Sb-1Ag solder joint and from 0.85 µm to 1.63 µm for the 42Sn-Bi-1Sb-1Ag solder joint.

The stress-strain curves are compared across different alloy compositions and aging conditions in Figure 8. The most important result is that isothermally aged solder joints have a higher saturation stress than their as-reflowed counterparts, regardless of their alloy composition. Both Ag and Sb additions both are shown to increase the saturation stress of the eutectic alloy, with Ag having a more pronounced effect than Sb, likely due to the presence of Ag_3Sn particles. It can be seen that the 0.5 wt% Sb addition produces a lower saturation stress compared with the 1 wt% Sb addition one. This can be explained by what was observed in the microstructure analysis. The 0.5 wt% Sb samples have no SnSb IMC particle form in the solder joint, thus relying solely on the solid solution strengthening provided by the solute Sb atoms. In contrast, the 1 wt% Sb samples have fine SnSb IMC particles, though unevenly distributed, in the solder joint, providing second phase strengthening.

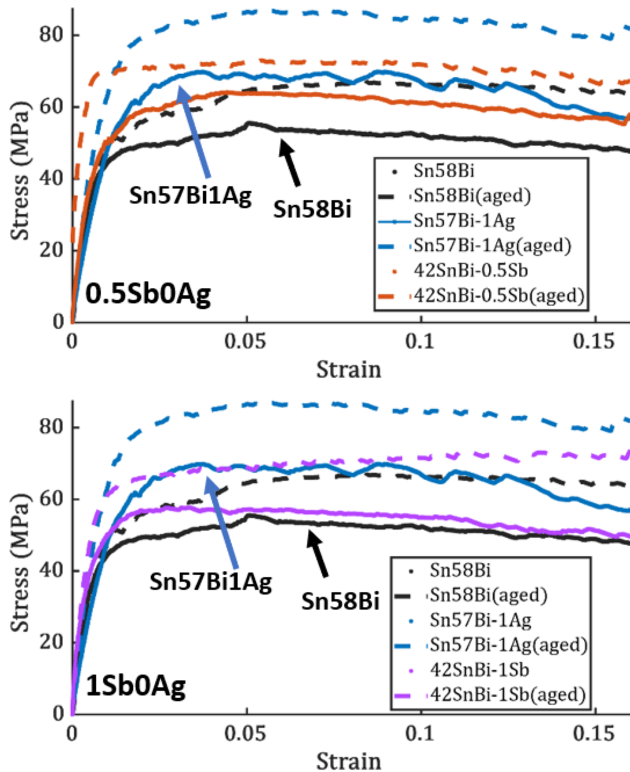

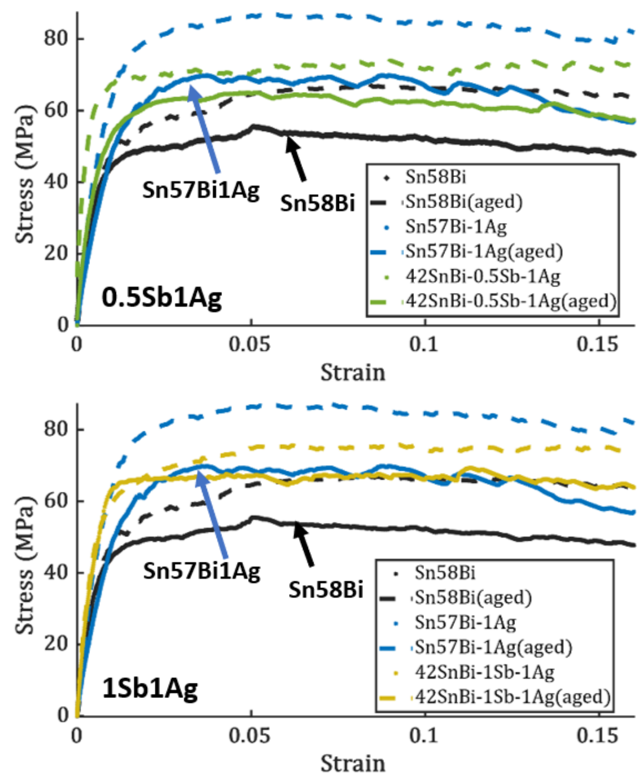

Figure 8. Stress-strain curves of monotonic shear testing at 30°C of as-reflowed and isothermally aged (85°C, 10 days) Four graphs are used to make it easy to compare Sn58Bi (unaged and aged) and Sn57Bi-1Ag (unaged and aged) with the four Sb-containing alloys 42SnBi-0.5Sb, 42SnBi-0.5Sb-1Ag, 42SnBi-1.0Sb, and 42SnBi-1.0Sb-1Ag in the unaged and aged conditions.

The Sb-containing samples performed well during mechanical testing despite the greater IMC layer thickness when compared to the eutectic 42Sn-Bi-1Ag samples and the IMC layer growth does not seem to negatively affect the mechanical properties of the solder joints in shear.

Conclusions

The microalloying effect of Sb and Ag on the thermodynamic, microstructural, and mechanical properties of near eutectic Sn-Bi alloys was examined. The addition of Sb is shown to increase both the melting and solidification temperature of the alloy, though at different rates and for different reasons. The Sb concentration impacts the microstructure of the Sn-Bi alloy in terms of both IMC formation and Sn dendrite morphology. With 0.5 wt% Sb addition, no SnSb forms and the as-reflowed microstructure shows fine and numerous Sn dendrites. Fine SnSb IMC particles form within the primary (Sn) phase in the 1 wt% Sb samples, while relatively large (>20µm) SnSb particles can be seen in the 2 wt% Sb samples. As the Sb concentration increases and the size of the primary SnSb particles increase, the Sn dendrites forming during solidification are fewer but coarser. Based on observations made on the microstructures, we propose that the reduced degree of undercooling at higher concentrations of Sb is a result of large, primary SnSb

particles serving as nucleation sites for Sn. The addition of Ag has a less pronounced effect on the thermodynamic behavior of the alloy.

In terms of the improvement on the mechanical properties of the alloys, the addition of Ag shows a more pronounced effect, which is likely due to the formation of Ag_3Sn IMC particles. Of the Sb-containing alloys tested, the 42Sn-Bi-1Sb solder had a higher saturation stress compared to the 42Sn-Bi-0.5Sb solder. This can be explained by the lack of precipitation strengthening in the 0.5 wt% Sb case. Aging increased the saturation stress for all the alloys, a surprising result, given that SAC alloys and SnPb typically age-soften. The ductility of these alloys cannot be quantified due to the limits of the mechanical testing set-up where the maximum strain achieved is 0.16, but the results show promising behavior with respect to the effects of Sb on microstructural stability and the effects of aging on stress-strain behavior in LTS alloys as a class.

Acknowledgements
This work was supported by the Semiconductor Research Corporation (SRC). We acknowledge additional support from the US Department of Defense [Contract No. W52P1J-22-9-3009]. The views and conclusions contained in this document are those of the authors and should not be interpreted as representing the official policies, either expressed or implied, of the US Department of Defense or the US Government. The US Government is authorized to reproduce and distribute reprints for Government purposes, notwithstanding any copyright notation herein.

References
1. Mokler S, Aspandiar R, Byrd K, Chen O, Walwadkar S (2016) The application of Bi-based solders for low temperature reflow to reduce cost while improving SMT yields in client computing systems
2. Hasnine, Md, et al. "Nanomechanical Characterization of SAC Solder Joints-Reduction of Aging Effects Using Microalloy Additions." *2015 IEEE 65th Electronic Components and Technology Conference (ECTC)*. IEEE, 2015.
3. Zhang, Yifei, et al. "The effects of SAC alloy composition on aging resistance and reliability." *2009 59th Electronic Components and Technology Conference*. IEEE, 2009.
4. Sakuyama S, Akamatsu T, Uenishi K, Sato T (2009) Effects of a Third Element on Microstructure and Mechanical Properties of Eutectic Sn-Bi Solder. Transactions of The Japan Institute of Electronics Packaging 2:98–103. https://doi.org/10.5104/jiepeng.2.98
5. Fowler HN, Tay SX, Blendell J, Handwerker CA (2023) Microalloying effects of Sb and Ag on the microstructural evolution of eutectic Sn–Bi alloys. MRS Advances 2023 1–5. https://doi.org/10.1557/S43580-022-00472-3
6. Yang F, Zhang L, Liu Z-Q, Zhong S-J, Ma J, Bao L (2016) Properties and Microstructures of Sn-Bi-X Lead-Free Solders. https://doi.org/10.1155/2016/9265195
7. Wang Z, Zhang QK, Chen YX, Song ZL (2019) Influences of Ag and In alloying on Sn-Bi eutectic solder and SnBi/Cu solder joints. JOURNAL OF MATERIALS SCIENCE-MATERIALS IN ELECTRONICS 30:18524–18538. https://doi.org/10.1007/s10854-019-02206-y
8. Mccormack M, Chen HS, Kammlott GW, Jin S (1997) Significantly improved mechanical properties of Bi-Sn solder alloys by Ag-doping. J Electron Mater 26:954–958. https://doi.org/10.1007/S11664-997-0281-7
9. Mokhtari O, Nishikawa H (2016) Correlation between microstructure and mechanical properties of Sn-Bi-X solders. Materials Science and Engineering A 651:831–839. https://doi.org/10.1016/j.msea.2015.11.038
10. Zhang C, Zhou J, Liu S-D, Qian G-T, Xue F (2014) Effect of Sb content on properties of Sn−Bi solders. Trans Nonferrous Met Soc China 24:191. https://doi.org/10.1016/S1003-6326(14)63046-6
11. Wang F, Chen H, Huang Y, Liu L, Zhang Z (2019) Recent progress on the development of Sn–Bi based low-temperature Pb-free solders. Journal of Materials Science: Materials in Electronics 30:3222–3243
12. da Silveira AF, de Castro WB, Luciano BA, Kiminami CS (2004) Microstructure of under-cooled Sn-Bi and Al-Si alloys. Materials Science and Engineering A 375–377:473–478. https://doi.org/10.1016/J.MSEA.2003.10.017
13. Subramanian, K. N., & Swenson, D. (2007). The effects of suppressed beta tin nucleation on the microstructural evolution of lead-free solder joints. Lead-Free Electronic Solders: A Special Issue of the Journal of Materials Science: Materials in Electronics, 39-54.
14. P.L., S. A., Greene, C. v., Lai, S. Y., Radulescu, R., Fowler, H., Blendell, J., Handwerker, C., Subbarayan, G., & Badwe, N. (2023). Comparative Mechanical Behavior of Sn-Bi based Low Temperature Solder Alloys under Different Pretest Aging Conditions. 2023 IEEE 73rd Electronic Components and Technology Conference (ECTC), 2218–2222. https://doi.org/10.1109/ECTC51909.2023.00384
15. Andersson, J. O., Helander, T., Höglund, L., Shi, P. F., & Sundman, B. (2002). Thermo-Calc 2023a, TCSLD4: Solder Alloys v4.2, Computational tools for materials science. Calphad, 26, 273–312.
16. Paixão JL, Gomes LF, Reyes RV, Garcia A, Spinelli JE, Silva BL (2020) Microstructure characterization and tensile properties of directionally solidified Sn-52 wt% Bi-1wt% Sb and Sn-52wt% Bi-2wt% Sb alloys. Mater Charact 166:110445. https://doi.org/10.1016/j.matchar.2020.110445
17. Wu, Y., Fowler, H. N., Weddington, N., Blendell, J. E., & Handwerker, C. A. (2023). Effect of Sb and Ag additions on the melting and solidification of Sn-Bi solder alloys. *MRS Advances*, 1-5.